Polymer Chemistry

Accepted Manuscript

ROYAL SOCIETY OF CHEMISTRY

www.rsc.org/polymers

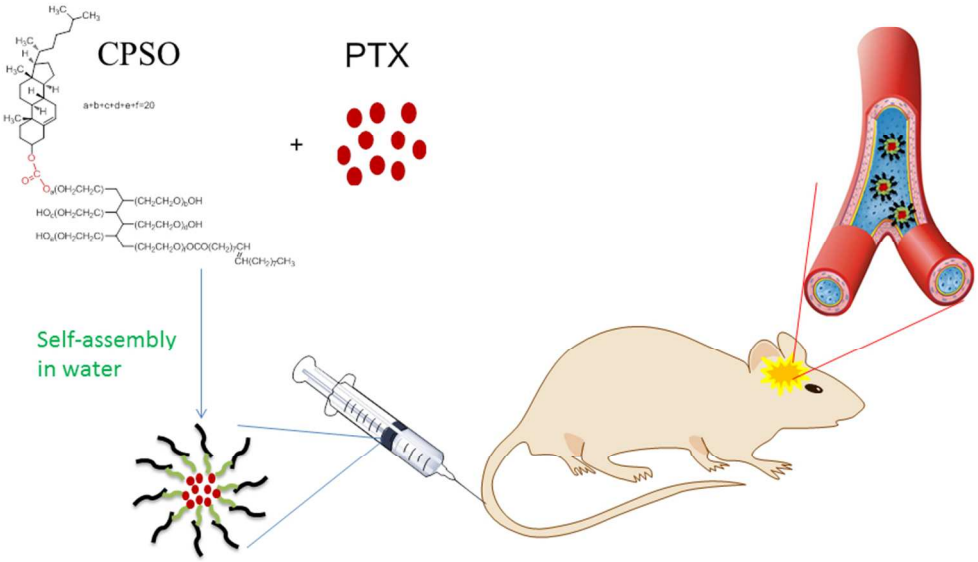

254x190mm (96 x 96 DPI)

Journal Name

RSCPublishing

ARTICLE

Paclitaxel-loaded Cholesterol-conjugated Polyoxyethylene Sorbitol Oleate Polymeric Micelles for Glioblastoma therapy across Blood-Brain Barrier

Cite this: DOI: 10.1039/x0xx00000x

Received 00th January 2012,
Accepted 00th January 2012

DOI: 10.1039/x0xx00000x

www.rsc.org/

Chang Li[a, b], Shasha Li[a], Taojian Tu[a] , Xingxing Qi[a], Yerong Xiong[a], Shuang Du[c], Yan Shen[a], Jiasheng Tu[a, *], Chunmeng Sun[a, *]

In this study, a brain delivery system was engineered by conjugation of cholesterol to polyoxyethylene sorbitol oleate (CPSO) to obtain an amphipathic copolymer, which could facilitate the transport of the self-assembled CPSO micelles across the blood-brain barrier (BBB). The CPSO micelles possessed satisfactory physicochemical properties, such as mean particle size at around 170 nm and drug loading at ~20%. It was also proved that CPSO was safe enough for intravenous injection according to the results from MTT assay, hemolysis rate, vascular stimulation and pathological sections studies. Fluorescent trafficking study showed that the CPSO could significantly accumulate in U87 cells and release payloads in endolysosomes. From pharmacodynamics study, paclitaxel (PTX)-loaded CPSO micelles could bring about significant tumor inhibition and prolong the median survival times compared to saline and Taxol® groups. What's more, both *in vitro* and *in vivo* results revealed that the CPSO exhibited an enhanced capacity to cross the BBB compared to Taxol®. These data indicated that CPSO micelles, as a safe and biocompatible drug delivery system, could be a promising carrier candidate for delivery of chemotherapeutics and/or diagnostics into brain tumors.

Keywords: Blood-brain barrier; Polymeric micelles; Cholesterol; Polyoxyethylene sorbitol oleate; Paclitaxel

Introduction

Glioblastoma (GBM) is the most prevalent and malignant primary central nervous system tumor in adults. Although a large number of advanced treatment paradigms have had impacts on medical management for many tumors, prolonging GBM patients' survival has not been achieved in the past decades. The median survival time of glioblastoma patients is only up to months. By reason of the difficulty in complete surgical excision, combination of irradiation and chemotherapy plays an important role in conventional GBM treatment [1-3]. But the effectsof chemotherapy on GBM are very limited as a result of poor drug accumulation in tumor sites due to the blood-brain barrier (BBB) [4]. A basal membrane and brain cells, such as pericytes and astrocytes, surrounding the endothelial cells further form and maintain an enzymatic and physical barrier that regulates the passage of molecules from the systemic circulation to the brain parenchyma known as the BBB [5]. Only un-ionized, lipophilic and low molecular weight molecules can diffuse

freely through the endothelial membrane and may thus passively cross the BBB [6]. While the BBB constitutes a natural defense mechanism that safeguards the brain against the invasion of various circulating toxins and infected cells, it also offers one of the most exclusive biological barriers limiting the brain uptake of diagnostic and/or therapeutic agents [7].

Nanoparticle systems, such as polymer micelles and nanocomplex, have been widely used for targeted carcinoma therapy [8-11]. Meanwhile, some reports declared that the nanoparticles, especially those coated with polysorbate 80, could also cross BBB to achieve GBM-targeted drug delivery [12-16]. However, the use of polysorbate 80 as a drug excipient has been recently implicated in adverse clinical effects, including acute hypersensitivity and hemolytic reaction [17]. The acute hypersensitivity triggered by polysorbate 80 is usually considered as a non-immune anaphylactic reaction, namely pseudoallergy. Pseudoallergy is a reaction similar to immune allergic reactions which can be observed following the first administration of offending agents. Unlike common allergies, pseudoallergic reactions can directly induce the release of histamine from mast cells and activate the complement system which are not initiated or mediated by pre-existing IgE antibodies [18]. Pseudoallergy has also been reported in a number of medicines containing polysorbate 80, including docetaxel, paclitaxel, omalizumab and etoposide. To overcome the side-effects, polyoxyethylene sorbitol oleate (PSO), based on polysorbate 80 containing a homogenous sorbitol matrix, was developed with improved safety against polysorbate 80. Furthermore, the critical quality attributes (CQAs) of PSO were similar to the commercial polysorbate 80 [9].

Following our previous investigations, we herein generated a novel brain delivery system on the basis of cholesterol-conjugated PSO (CPSO) that could be used as a safe and biocompatible carrier of PTX for GBM therapy. The engineered CPSO micelles wer expected to be stable in bloodstream and cross the BBB. The localization of micelles in U87 human GBM was observed by fluorescent probe technique and *in vivo* imagine. The drug-loading capacities and physicochemical characteristics of micelles were investigated in detail. The *in vitro* drug release study was evaluated in different pH environments. LysoTracker Red, a fluorescence probe, was encapsulated in micelles and the intracellular release was observed based on confocal microscopic analyses. The antitumor effect against GBM were compared among PTX-loaded CPSO, saline and Taxol®.

Experimental

Materials and Animals

Polyoxyethylene sorbitol oleate was obtained from Nanjing Well Chemical Corp. Ltd. (Nanjing, China). Cholesteryl Chloroformate was purchased from Aladdin (Shanghai, China). 4-dimethylaminopyridine (DMAP) was obtained from Aladdin (Shanghai, China). LysoTracker Red was purchased from Invitrogen Corporation (Carlsbad, USA). DiR was obtained from Biotium (California, USA). Dialysis bags (MWCO=1000 and 2000) were purchased from Spectrum (USA). DAPI was obtained from Invivo Gen (California, USA). Paclitaxel was purchased from Natural Field Bio-technique Co. Ltd. (Xi' an, China). All other chemicals were from various suppliers and were reagent grade or better.

Normal mice, SD rats and New Zealand rabbits were purchased from Qinglong Mountain farm, Nanjing, China. Fluorescent U87 cells-bearing in situ nude mice were purchased from Source Biotechnology Co. Ltd., Nanjing, China. All animal experiments were implemented according to the National Institute of Health Guide

for the Care and Use of Laboratory Animals and approved by the Animal Ethics Committee of China Pharmaceutical University.

Cell culture

Primary rat brain microvascular endothelial cells (RBMECs) were obtained from 7-day old rats. The cells were maintained in RPMI 1640 supplemented with fetal calf serum (20%), penicillin and streptomycin (100 U/mL), cultured in an incubator at 37 ℃ in a humid atmosphere of 5% CO_2. U87 and RBL-2H3 cells were maintained in monolayer culture in Eagle's minimum essential medium with 15% fetal bovine serum and 1% penicillin/streptomycin under an atmosphere of 5% CO_2 at 37 ℃.

Synthesis of cholesterol-conjugated polyoxyethylene sorbitol oleate (CPSO)

Chloroform, proportional cholesteryl chloroformate and polyoxyethylene sorbitol oleate were mixed and reacted at room temperature for 24 h using DMAP as the catalyst. Chloroform was then removed by rotary evaporation, and reaction products were dissolved in de-ionized water and centrifuged at 3000 rpm for 15 min to remove impurities. The supernatant was then lyophilized to obtain CPSO [19].

Preparation and characterization of CPSO and PTX-CPSO micelles

To prepare CPSO micelles, appropriate amount of CPSO conjugates were dissolved in distilled water and then sonicated for 15 min using a probe type ultrasonicator (JY 92-2D, Ningbo Scientz Biotechnology Co., Ltd, Zhejiang, China) in an ice bath. For preparation of PTX-CPSO micelles, PTX dissolved in ethanol was dropwise added into CPSO solution. The mixture was sonicated for 30 min in an ice bath. The solution was dialyzed overnight against 4 L of distilled water (dialysis bag MWCO = 1000 Da), followed by centrifugation at 3000 rpm for 15 min. The supernatant was subsequently filtered through a 0.45 μm microporous membrane and lyophilized.

The transmission electron microscopy (TEM) images, atomic force microscopy (AFM), critical micelle concentration (CMC) assay and drug-loading (DL) were measured following previously published methods [20-21]. The DL was calculated by the following equation:

$$DL\ (wt\%) = \frac{weight\ of\ PTX\ in\ micelles}{weight\ of\ PTX\ in\ micelles + weight\ of\ CPSO\ added\ initially} \times 100$$

Our *in vitro* blood-barrier model consists of rat brain microvascular endothelial cells (RBMECs) cultivated for seven days on cell culture inserts. The inserts were coated with gelatin to enable the formation of a RBMECs monolayer. In previous studies, RBMECs have already been used as an *in vitro* BBB model and it was shown that this model exhibit similar brain endothelial cell characteristics [22]. To determine the density and integrity of the BBB model, two different methods were applied: 1) morphological observation using optical microscope; 2) trans-endothelial electrical resistance (TEER) determination of the RBMECs monolayer membrane.

Normal mice and fluorescent U87 cells-bearing in situ nude mice were injected with DiR loaded CPSO micelles and free DiR (200 μg/kg) *via* the tail vein and then anesthetized using intramuscular injection of chloral hydrate (20 mg/kg). *In vivo* imaging experiments were performed at 0.5, 3, 6 and 24 h post injection using a Kodak multimodal imaging system IS2000MM (Kodak, USA) equipped with an excitation band pass filter at 365 nm and an emission cut-off filter at 790 nm. Images were analyzed using the imaging station IS2000MM software (Kodak ID Image Analysis Software; Kodak) [23].

***In vitro* stability and drug release at different pH**

values

The serum stability assay *in vitro* was performed according to the method described previously [24]. To mimic the in vivo microenvironment, Taxol® and PTX-CPSO micelles were incubated in the presence of FBS for 12 h, while PTX-CPSO incubated without serum was set as the control group. At designated time points, 100 μL supernatant was withdrawn, filtered through a 0.45 μm microporous membrane, and centrifuged at 3000 rpm for 15 min. The stability of micelles in tumor tissue was performed as follows: 1 mg/mL PTX-CPSO micelles solution was mixed with U87 tumor tissue fluid at series of volume ratios of 10%, 50% and 90%; at the designated time points, 100 μL supernatant was withdrawn, filtered through a 0.45 μm microporous membrane and centrifuged at 3000 rpm for 15 min. The content of PTX in each collected sample was detected by HPLC (Shimadzu, Japan).

The release profiles of PTX from micelles were conducted by a dialysis method . Two milliliters of PTX-CPSO micelles solution containing 2 mg of PTX were placed in a dialysis bag (MWCO 2000 Da) and submerged in 200 mL PBS at different pH values, i.e., 4.5, 5.8 and 8.4, and gently shaken in a water bath at 90 rpm and 37 □ (SHZ-28A temperature controlled oscillation instrument, Taicang Experimental Company, Suzhou, China). One milliliter PBS was withdrawn at predetermined time points and immediately replaced with equivalent fresh PBS. The content of PTX was also detected by HPLC (Shimadzu, Japan).

Intracellular uptake and distribution of micelles and intracellular delivery efficiency of Lyso Tracker Red

To identify the cellular uptake kinetics of CPSO micelles, the cellular uptake of coumarin 6 was measured using fluorescence microscopy and flow cytometry at different time points (30, 60 and 240 min). The U87 cells (10^5 cells/well) were seeded on 6-well plates (Costar, USA) and cultured at 37 □ for 24 h. After incubation with micelles, the cells were treated and the qualitative and quantitative fluorescence intensity of coumarin 6 was analyzed using fluorescence microscope and flow cytometry.

Intracellular location of CPSO micelles was investigated using confocal laser scanning microscopy (CLSM). U87 cells were cultured in 35 mm glass bottom culture dishes for 24 h. The media were then replaced with 1 mL of the media containing coumarin 6 (100 nM)-loaded complexes. After incubation at 37 □ for 6 h, the culture media were subsequently removed and the cells were rinsed with PBS for three times. The cells were fixed with 4% paraformaldehyde, and DAPI (final concentration 10 mg/mL) was added to stain the cell nuclei for 10 min before imaging. Intracellular location of CPSO was observed using a confocal microscope (Leica TCS SP5, Heidelerg, Germany). Fluorescence was excited at 466 nm and 358 nm, and emitted at 504 nm and 461 nm for coumarin 6 and DAPI, respectively. The images were analyzed using Leica CLSM software [25].

To discern the endosomal/lysosomal escape for efficient intracellular trafficking, the double labeling experiments were performed using CLSM for observing the cytoplasmic distribution of CPSO micelles on U87 cells. The localization of coumarin 6-loaded CPSO micelles was visualized by labeling cells with the specific fluorescent probe, i.e., LysoTracker Red. The cells (10^5 cells/well) were seeded in 35 mm glass bottomed dishes and cultured at 37 □ for 24 h. The cells were incubated with coumarin 6-CPSO micelles (100 ng/mL based on coumarin 6). At prearranged time intervals (1, 4, 8 h), the cells were washed twice with cold PBS and then stained with 50 nM LysoTracker Red for 30 min at 37 □. The cells were washed twice with

cold PBS and observed immediately without fixing by CLSM [25-26].

In vitro cytotoxicity and PTX-induced U87 apoptosis assay

In vitro antiproliferative activities of PTX-loaded CPSO micelles and Taxol® against U87 cells, and the cytotoxicity of blank CPSO and ethanol: EL 35(1/1) were estimated by MTT assay. The cells were seeded at a density of 10^4 cells per well in 96 well plates for 24 h. The cells were exposed to the culture medium (FBS free) containing various concentrations of the different formulations for 24 h. 20 μL MTT (5 mg/mL) was added to each well followed by incubation for another 4 h. Then the medium was replaced with 200 μL DMSO. Following agitation for 10 min, the viable cells were quantified by recording the UV absorbance at 490 nm on a microplate reader (BioTek, USA).

Cells apoptosis was first identified morphologically by DAPI staining. Briefly, U87 cells were seeded into a 35 mm glass bottom culture dish at a density of 10^5 cells/well and cultured at 37 □ for 24 h. Cells were then incubated for another 24 h with Taxol®, PTX-CPSO micelles (PTX concentration of 100 ng/mL) or blank culture medium. Samples were then fixed with 4% paraformaldehyde in PBS for 10 min, stained with DAPI (10 μg/mL) in PBS for 15 min and washed twice with cold PBS, and examined under the fluorescence microscope.

U87 cells seeded in the 6 well plates were treated with Taxol® and PTX-CPSO micelles (PTX concentration of 100 ng/mL) at 37 □ for 24 h. Cells treated with FBS-free culture medium were served as control. At the end of incubation, adherent and non-adherent cells were trypsinized. Cells (10^6) were collected by centrifugation at 1000 g for 5 min, washed twice with cold PBS and fixed with 70% cold ethanol and stored at 4 □ for 24 h. Cells were centrifuged again and washed with cold PBS twice, followed by staining with PI (0.1 mg/mL) for 30 min. The DNA content was measured by flow cytometry and the percentage of cells in each phase of the cell cycle was evaluated using the ModFit software.

In vitro hemolysis, vascular irritation and pseudoallergy studies

The hemolytic study was performed according to the method described previously [9]. Blood was drawn from anesthetized New Zealand rabbits by cardiac puncture, and centrifuged at 3000 rpm for 10 min immediately. The collected red blood cells (RBCs) were washed with physiological saline, and then suspended in physiological saline to a concentration of 2%. Aliquots of 2% RBC suspension containing the tested carriers with different concentrations ranging from 0.01 to 0.2 mg/mL were incubated at 37 □ for 1 h. The positive and negative controls were water and physiological saline, respectively. The samples were then centrifuged at 3000 rpm for 10 min to remove non-lysed RBC. The supernatant was collected and analyzed by microplate reader at 540 nm (BioTek, USA). The hemolysis rate was determined by the following formula:

$$\text{Hemolysis (\%)} = \frac{A_{sample}-A_{negative}}{A_{positive}-A_{negative}} \times 100$$

To investigate the vascular irritation, the New Zealand rabbits were injected in the auricular veins with different formulations at a dose of 10 mg/kg once per day for three days. The injection speed was 1 mL/min. After a recovery phase of 24 h, the rabbits were sacrificed and the auricular vein tissues were examined for pathological assay.

β-hexosaminidase release assay was performed for *in vitro* evaluation of pseudoallergy as described elsewhere [9]. In brief, confluent RBL-2H3 cells were seeded in 96-well plate. Then the cells attached to microtiter wells were washed

twice with Tyrode's buffer and the stimulation was initiated by adding 200 μL Tyrode's buffer containing CPSO, Taxol or PTX-CPSO micelles (1%, w/w). After 1 h incubation at 37 □, the degranulation was terminated by placing the plates on ice. To determine the amount of β-hexosaminidase released from the cells, 60 μL of supernatant and 60 μL of β-hexosaminidase substrate solution (5mmol/mL p-Nitrophenyl-2-acetamido-2-deoxy-beta-D-glucopy-ranoside in 0.1 mol/mL sodium acetate buffer, pH 4.5) were mixed in a new 96-well plate and incubated for 1 h at 37 ℃. Subsequently, 150 μL carbonate buffer containing 100 mmol/L $NaCO_3$ and 100 mmol/L $NaHCO_3$ buffer at pH 10.7 were added into wells to quench the reaction. The negative control group incubated with only Tyrode's buffer was determined to assess spontaneous β-hexosaminidase release. Total β-hexosaminidase amount was obtained by lysing the cells with 0.1% Triton-X 100 prior to the supernatant removal. β-hexosaminidase in the supernatant was quantified by measuring the absorbance at 450 nm using ELx800 microplate reader (BioTek Instruments, USA). The background absorbance of substrate in Tyrode's buffer alone (no cell supernatant) was subtracted from all readings before plotting.

In vivo distribution and antitumor efficacy

To assess the effect of PTX-loaded CPSO micelles on biodistribution and brain targeting ability of PTX, normal mice were randomly divided into two groups. Mice were administered intravenously a single dose of PTX (20 mg/kg) in the form of Taxol® and PTX-CPSO micelles. After 10 min, 30 min, 2, 4, 8, 12, 24 and 48 h of injection, the mice were sacrificed by cervical dislocation in order to obtain tissue samples. The organs (brain, heart, liver, spleen, lung and kidney) were removed and washed twice with physiological solution (0.9% NaCl), weighed and stored at -20 □ until analysis. The concentration of PTX from each tissue homogenate was measured by HPLC (Shimadzu, Kyoto, Japan) as described previously [27].

U87 cells-bearing mice model were established and randomly assigned to 3 groups. Once the volume of tumor under oxter was grown to approximately 50 mm^3, treatments were administered *via* the tail vein at a dose of 3 mg/kg and given every five days for 5 times. Tumor growth in the U87-bearing mice was measured with a vernier caliper. Thereafter, tumor volumes were calculated as follows:

$$V = L \times S^2 \times 0.5$$

Where V is the volume of tumor, L is the longer diameter of tumor and S is the shorter diameter of tumor.

The survival time and weight change of U87-bearing in situ mice model treated as above was also monitored. To further evaluate the safety of PTX-CPSO micelles, the harvested heart, liver and kidney were fixed in a phosphatebuffered formaldehyde solution, and embedded in paraffin. Histological sections (12 mm thickness) were achieved using a Freezing Microtome (Reichert HistoSTAT, USA). We randomly selected independent areas and took images using a bright-field microscope (Olympus, Japan) [28].

Statistical analysis

Data were expressed as means ± SD from triplicate experiments performed in a parallel manner unless otherwise indicated. The results were analyzed using an unpaired, two-tailed Student's t-test. All comparisons were made relative to corresponding controls and significance of difference was indicated as asterisk (*$P < 0.05$, **$P < 0.01$, ***$P < 0.001$).

Results and discussion

Synthesis and Characterization of CPSO

micelles

The CPSO product was creamy-white and waxy. Representative TEM and AFM images of the resulting blank and PTX-loaded CPSO micelles were shown in Figure 1A, B and C, while the particle size distribution, zeta potential and drug loading in Table 1. In general, the drug-loaded micelles with ~170 nm average size could bring about better EPR effect [29]. We also investigated the particle size and zeta potential of DiR-loaded CPSO micelles. The results showed that the DiR-CPSO micelles owned similar particle size at ~164 nm compared to PTX-CPSO micelles. The CMC of amphiphilic CPSO was 5.74 mg/L (Figure 1D) which was calculated by fluorescence spectroscopy using pyrene as a probe. Such low CMC value guaranteed that the self-assembled micelles were able to retain their original morphology under highly diluted conditions before approaching the targeting sites.

Table 1. Characteristics of blank CPSO, PTX-loaded and DiR-loaded CPSO micelles. The values are expressed as mean ± S.D.

Samples	Size (nm)	Zeta potential (mV)	Drug Loading (%)
CPSO	35.5 ± 0.6	-0.66 ± 0.65	/
PTX-CPSO	172.0 ± 1.8	-15.47 ± 0.44	20.48 ± 2.12
DiR-CPSO	164.1 ± 3.6	-13.84 ± 0.59	/

The dye coumarin 6 was loaded by CPSO as a drug model due to its easy detection using *a* fluorescence spectroscopy. We detected a significantly increased transport of coumarin 6 in the groups of polysorbate 80 and CPSO compared with ethanol/cremophor EL 35(1/1, v/v), as shown in Figure 1E. It was demonstrated that CPSO could permeate across the *in vitro* BBB model. The morphological characteristics and resistance data of *in vitro* BBB model are shown in Figure S1 A and B (Supporting Information).

Moreover, the *in vivo* biodistribution of blank micelles in normal mice was investigated qualitatively by a non-invasive near infrared optical imaging technique. The mice receiving DiR-CPSO micelles and free DiR were imaged at 0.5 h, 6 h and 24 h post-injection. During the *in vivo* imaging test, most of the DiR fluorescence accumulated in liver 6 h after intravenous administration of free DiR, yet, in CPSO group, strong fluorescent signals could be observed in brain up to 24 h after injection, which provided the decisive evidence that our CPSO micelles were efficient for brain targeted drug delivery. Moreover, NMR, UV/vis, IR and DSC analysis of CPSO were performed (Figure S2 A, B and Figure S3 A, B and C in Supporting Information).

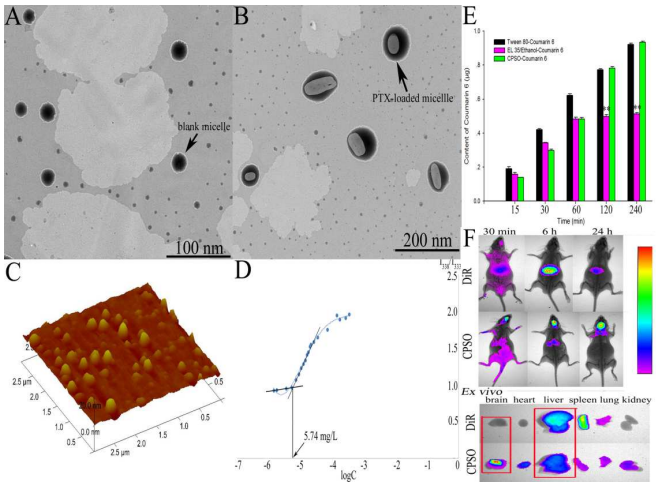

Fig. 1. TEM images of blank CPSO micelles (A) and PTX-loaded CPSO micelles (B); AFM image of PTX-loaded micelles (C); CMC value of CPSO micelles (D); The results of *in vitro* transmembrane study in BBB model. The data were shown as mean ± S.D. ** indicates a significant difference ($P < 0.01$) versus CPSO (E); *In vivo* biodistribution of CPSO micelles in normal mice at different time points (F).

In vitro stability and drug release at different pH values

To further investigate the effect of the destabilization of the hydrophobic core upon release, we assessed the stability of CPSO micelles in the presence of serum or tumor tissue fluid. As shown in Figure 2A, the PTX-loaded CPSO micelles exhibited the best stability in serum environment. After 12 h incubation with or without serum, the PTX loading of CPSO micelles was 4.1-fold and 3.5-fold than that of Taxol®, respectively, indicating that the negative zeta potential was able to greatly stabilize PTX-loaded micelles. Figure 2B showed that PTX-loaded CPSO micelles also exhibited great stability in ex vivo tumor environment. The content of PTX remained 80%, 60% and 50% in 10%, 50% and 90% *ex vivo* tumor tissue fluid, respectively. It was demonstrated that before the micelles accumulated in tumor through EPR effect, most micelles kept their integrity in blood circulation. The particle size of micelles turned to 204.2 ± 9.8 nm, 250.3 ± 8.3 nm and 316.3 ± 15.9 nm after incubation with 10%, 50% and 90% *ex vivo* tumor tissue fluid, respectively.

The pH-responsive PTX release from CPSO micelles was also evaluated. Figure 2C showed the release of PTX from micelles against PBS (1% Tween 80) at pH 7.4, 5.8 and 4.5 at 37 ℃. Inefficient and slow release of PTX from CPSO micelles was observed at pH 7.4. For example, only 8.1% of PTX was released in the first 8 h and approximately 20% released within 144 h, whereas about 53.2% and 65.0% of PTX could be released in 144 h at pH 5.8 and 4.5, respectively, reflecting the release of PTX was accelerated at lower pH conditions, where the hydrolysis of carbonic ester linkage could take place [19].

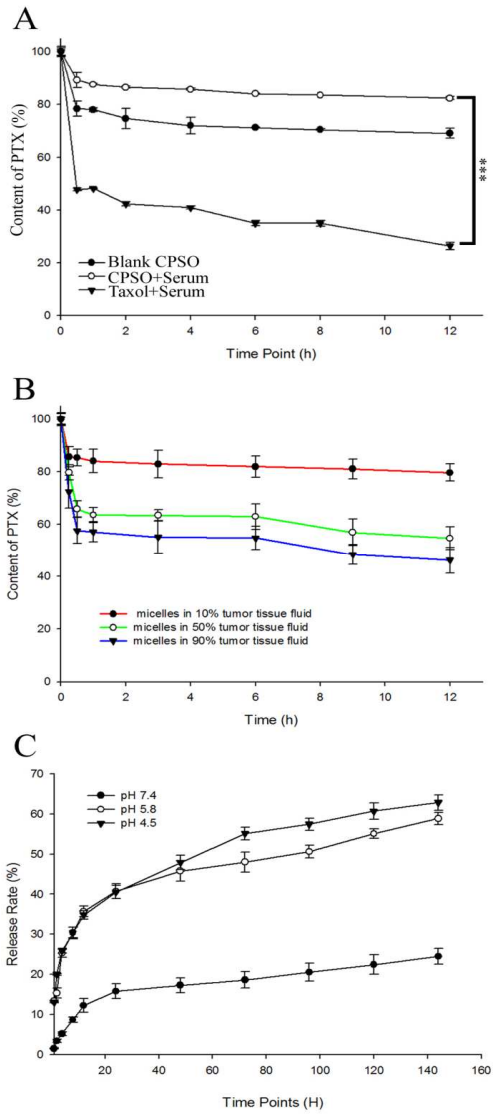

Fig. 2. The stability of PTX-loaded CPSO micelles in presence of serum (A) and tumor tissue fluid (B). The *in vitro* release plot at different pH values (C).

Intracellular uptake of coumarin 6-loaded micelles

Afterwards, we investigated the cellular uptake of micelles and intracellular release of encapsulated payloads using coumarin 6 as fluorescent marker. The result of intracellular uptake was examined qualitatively and quantitatively, as shown in Figure 3A and B. Strong green fluorescence was observed when U87 cells were incubated with CPSO micelles for 30 min, 1 h and 4 h. Commercial polysorbate 80 was used as a control. It was observed that the mean coumarin 6 green

fluorescence intensity for CPSO micelles were approximately 1.2-fold and 1.5-fold compared to those of polysorbate 80 after 1 h and 4 h of incubation, respectively. The higher fluorescence intensity of coumarin 6-loaded CPSO micelles implied greater intracellular uptake capability. Furthermore, it was demonstrated by CLSM that CPSO micelles were distributed in the cytoplasm. As shown in Figure 3C, green fluorescence of coumarin 6 dispersed homogeneously around the cell nucleus in blue. While the mechanism of PTX to inhibit mitosis is related to tubulin in the cytoplasm, our data give the evidence that PTX-CPSO could achieve efficient anti-tumor cure [30]. In this regard, the intracellular delivery of LysoTracker Red in U87 cells was further investigated using CLSM. Lysosomes and endosomes were observed as red fluorescence after the cells were stained with specific organelle-selective dyes, while coumarin 6/CPSO micelles were shown as green fluorescence. Co-localization of the micelles with the specific organelle dyes appeared yellow. As shown in Figure 3D, majority of the green fluorescence was highly overlaid with the yellow fluorescence when the cells were incubated with coumarin 6/CPSO for 1 h, demonstrating that the CPSO micelles were entrapped in the endosomes. After 4 h, the green fluorescence had a significant dissociation from the red fluorescence, reflecting the efficient endolysosomal escape of coumarin 6. At 8 h, coumarin 6/CPSO showed more efficient endolysosomal release and cytoplasmic distribution, similar to the result of intracellular distribution [26]. The mechanism of intracellular release from CPSO micelles is considered that the carbonic ester conjugated bond could be easily cleaved at acidic environment in the endolysosomes [19, 31], and the fluorescence dye or PTX will be released from micelles and consecutively accumulate in cytoplasm through free diffusion.

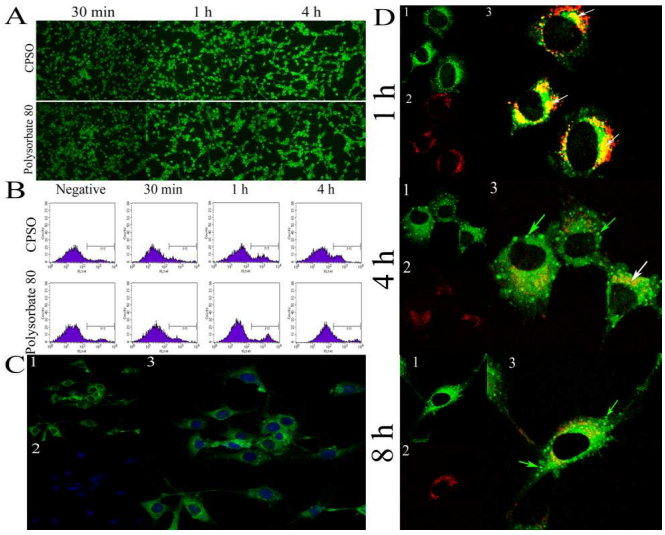

Fig. 3. Cellular uptake, intracellular location and delivery efficiency of CPSO evaluation in U87 cell line. Micrographs of U87 cells after the uptake of coumarin 6/CPSO and coumarin 6/polysorbate 80 for 30 min, 1 h and 4 h incubation (A); FACS analysis for cellular uptake of coumarin 6/CPSO and coumarin 6/polysorbate 80 (B); Confocal microscopic observations for intracellular location of coumarin 6/CPSO in U87 cells (C); Intracellular delivery of the micelles in U87 cells at different time observed by CLSM (D). The late endosomes and lysosomes were stained by LysoTracker Red. 1: green fluorescence represents coumarin 6; 2: red fluorescence represents endolysosomes; 3: overlay of 1 and 2. The white arrows indicate the occasions of coincidence between the CPSO micelles and endolysosomes. Green arrows indicate that coumarin 6 have escaped from endolysosomes into the cytoplasm.

In vitro cytotoxicity and PTX-induced U87 apoptosis assay

The cytotoxicity of Taxol®, ethanol/cremophor EL (1/1, v/v), blank CPSO micelles and PTX-loaded CPSO micelles in U87 cells were evaluated by MTT assay. As shown in Figure 4A, both Taxol® and PTX-loaded CPSO micelles caused concentration-dependent cell death. Drug-loaded CPSO micelles led to higher U87 cells apoptosis rate versus Taxol® at lower concentraitons of PTX (0.2 – 2 μg/mL), while the apoptosis rate of Taxol® was higher than that of PTX-loaded micelles at

PTX concentrations of 5 and 10 μg/mL. It is presumed that PTX in Taxol® formulation can be readily transported into cells and diffuse in cytosol by the passive diffusion mechanism at high concentrations [29] and the solubilizer in Taxol® (i.e., ethanol/cremophor EL (1/1, v/v)) possesses certain cytotoxicity. So the apoptosis of U87 cells was attributed to the synergistic effect of PTX as well as the solubilizer at high concentrations. In Figure 4B, the cytotoxicity of ethanol/cremophor EL (1/1, v/v) was significantly higher than that of blank CPSO micelles across the 0.002-200 μg/mL concentration range, which was consistent with the above hypothesis. Table 2 displayed the IC50 values of Taxol® and PTX-loaded CPSO micelles. The nuclei of untreated U87 cells showed homogenous fluorescence without segmentation and fragmentation after DAPI staining (Figure 4 C). In contrast, the cell nuclei became severely fragmented after the cells were treated with PTX formulations for 24 h, suggesting that the nuclei were segmented into dense nuclear parts and further distributed into apoptotic bodies. Compared with Taxol®, PTX-loaded micelles could induce more severe fragmentation of the cell nuclei. To measure the apoptotic effect of various PTX formulations quantitatively, Annexin V-FITC Apoptosis Detection kit was used to stain the U87 cells and the percentage of cell apoptosis was determined by flow cytometry as shown in Figure 4D. The percentage of early and late apoptosis of Taxol®-treated U87 cells was 13.44 ± 1.53% and 15.35 ± 0.94%, respectively. Compared with Taxol® injection, PTX-loaded CPSO micelles caused 27.47 ± 0.49% and 22.28 ± 0.51% for early and late cell apoptosis. These results were consistent with the observed results of cellular nucleus staining and in vitro MTT assay, indicating that PTX-loaded micelles produced higher cytotoxicity than Taxol®.

Table 2. Cytotoxicity of PTX in Taxol® and PTX-CPSO micelles against U87 cells. Values are presented as mean ± S.D.

Formulations	IC_{50} (μg/mL) for 24 h
Taxol®	0.854 ± 0.105
PTX-CPSO micelles	1.043 ± 0.225

In vitro hemolysis, vascular irritation and pseudoallergy studies

The hemolysis rate of CPSO was compared with that of ethanol/cremophor EL (1/1, v/v), the solubilizer of Taxol®. As shown in Figure 5A, the group of cremophor EL in 50% ethanol caused a concentration-dependent erythrocyte lysis, while CPSO only caused about 5% erythrocyte lysis even at the highest concentration. As reported previously [32], the hemolytic effect could be used to evaluate the membrane damage by carriers. Thus, the data implied that CPSO had a lower risk in membrane damage versus ethanol/cremophor EL (1/1, v/v). As shown in Figure 5B, physiological saline and PTX-loaded CPSO groups showed that the structure of vessels was intact and no inflammation, edema and thrombus were observed. However, there were serious thrombus and edema in the vascular system, and the structure of vessels was seriously damaged in Taxol® group. These results showed that the vascular irritation of drug-loaded CPSO micelles was significantly lower than that of Taxol®. To evaluate the CPSO-induced pseudoallergy *in vitro*, the amounts of β-hexosaminidase released from mast cells after treatment with CPSO and commercial products were determined and displayed in Figure 5C. Results revealed that the highest β-hexosaminidase release rate was detected in Taxol® group. After loading drug, PTX-loaded micelles led to higher β-hexosaminidase release compared to blank CPSO,

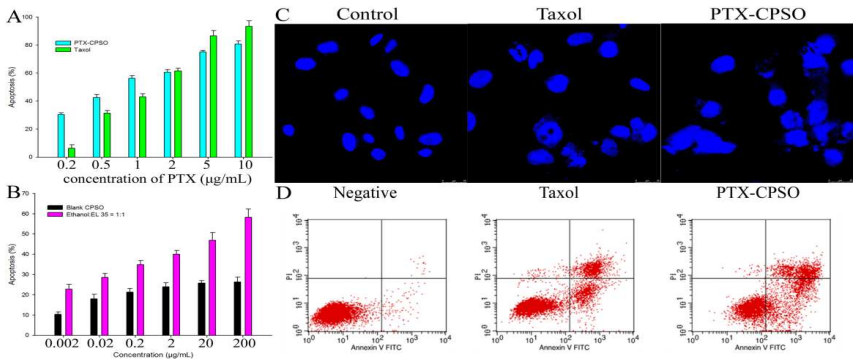

Fig. 4. Comparison of apoptosis between CPSO micelles and Taxol® with (A) or without (B) PTX. Fluorescence micrographs of U87 cells nuclei labeled by DAPI (C). Flow cytometry using the staining of Annexin V-FITC and PI (D).

indicating that PTX could trigger pseudoallergy to some extent. These results suggested that CPSO micelles were safe enough for intravenous administration.

In vivo imaging and tumor targeting study

To investigate the tumor passive targeting ability of CPSO micelles, the *in vivo* imaging in tumor-bearing nude mice was applied. Representative fluorescence images of living test and *ex vivo* brain test after administration of DiR-loaded CPSO micelles were shown in Figure 6. The fluorescent CPSO micelles initially spreaded in the whole body 30 min after injection (Data not shown), then accumulated increasingly in the brain tumors, where maximal fluorescence intensity could be observed at around 3 h. Tfluorescent signal in brain tumor could be still visible for up to 24h post-injection, indicating a remarkable retention of our CPSO micelles. After excision, brain samples were imaged under two wavelengths, 450 nm for U87 GBM cells and 720 nm for DiR. As shown Figure 6B, the overlaid fluorescent area indicated the accumulation of DiR/CPSO in tumor sites. These results suggested that after crossing the BBB, CPSO micelles could amply accumulate in the tumor tissues. It was demonstrated that the coat of polysorbate 80 was indispensable for BBB transport. Moreover, for brain targeting, other surfactants as coatings were proved to be less effective than polysorbate 80. The possible mechanism was presumed that nanoparticles coating with polysorbate 80 could be recognized as low-density lipoprotein (LDL) *in vivo*. They may adsorb ApoE which plays an important role in transportation of LDL into brain, so that the LDL receptor mediated endocytosis takes place [33-34]. As mentioned in previous section (Table 1), CPSO micelles loading PTX or DiR exhibited comparable particle size and zeta potential. Thus, it could be presumed that both CPSO micelles with different cargos would have similar effect in BBB crossing via LDL receptor mediated transport.

In vivo distribution and antitumor efficacy

To more precisely evaluate the *in vivo* distribution of PTX-CPSO micelles, the PTX amount in tissues (i.e., heart, liver, spleen, lung, kidney and brain) was measured after

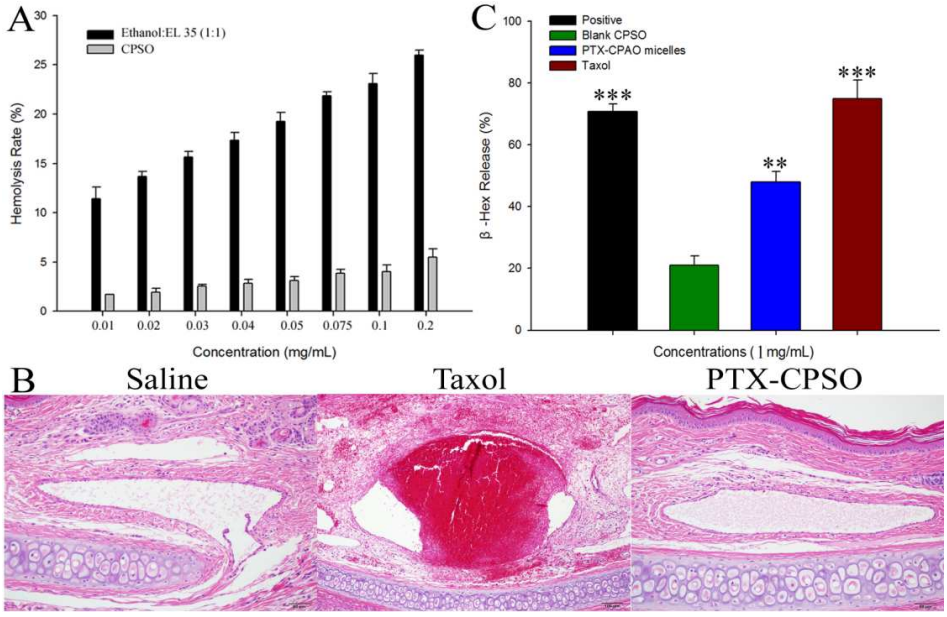

Fig. 5. The hemolysis rate of CPSO and ethanol: EL 35 (n = 3) (A). Study of stimulation in rabbit blood vessels after administration of saline, Taxol® and PTX-CPSO micelles (B). *in vitro* mast cells degranulation assay after incubation with different formulations (C). The data are shown as mean ± S.D. n = 5. Asterisk represents significantly statistical difference versus CPSO group (**P＜0.05, ***P＜0.001).

intravenous administration of PTX-loaded CPSO micelles and Taxol®. The results were presented in Figure 7A. Notably, the PTX concentration of PTX-CPSO micelles in the brain was significantly higher than that of Taxol® group from 2 h to 48 h. It was quantificationally demonstrated that CPSO micelles could cross the BBB *in vivo*. These data indicated that the injected micelles targeted and stayed in the brain for an extended time. PTX-CPSO micelles also exhibited higher accumulation in spleen and kidney for PTX, because of the "long-circulation" in the blood and a large amount of red blood cells (RBCs) stored in the spleen [35]. Additionally, the PTX-CPSO micelles were water-soluble so that they tended to be eliminated through kidney. Moreover, the PTX concentration in PTX-CPSO micelles in the heart, liver was significant lower than that of Taxol®, it was implied that the PTX-CPSO micelles could reduce the heart and liver toxicity caused by PTX.

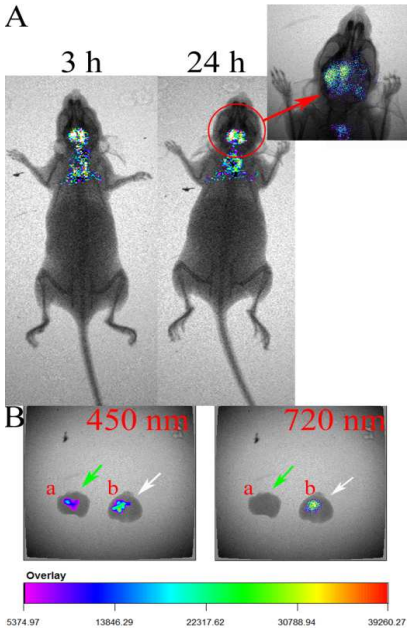

Fig. 6. *In vivo* non-invasive NIRF imaging of DiR loaded CPSO micelles in U87 tumor bearing nude mice at different time points (A); *ex vivo* images of the fluorescent U87 GBM tumor after administration of free DiR (a) and DiR-loaded CPSO micelles (b) at 450 nm and 720 nm (B).

In Figure 7B, an enhanced tumor inhibition effect was observed in the drug treatment groups. Owing to EPR effect and pH-responsive

intracellular trafficking, PTX-loaded CPSO micelles were able to significantly reduce tumor volumes by around 4.12-fold and 2.45-fold compared to saline and Taxol® groups, respectively. Taking the tumor targeting and accumulation effect of PTX-loaded CPSO micelles into account, the conclusion could be drawn that long-circulation effect *in vivo* was essential to concentrate high dose of chemotherapeutics in tumors, which depended on the extent of their extravasation to tumors, the degree of passive accumulation, and the circulation time of nanocarriers [36]. As shown in Figure 7C, the final tumor tissues were harvested and measured. The results revealed that PTX-CPSO micelles had the strongest efficacy on inhibiting tumor growth, and the inhibition rate calculated by tumor weight was about 60.14% for PTX-CPSO group, while 39.83% for Taxol® group. It could be found that the results in Figure 7B-D were in good agreement with each other. The therapeutic effects of different formulations were determined by comparing their respective survival times of tumor-bearing mice (Figure 7E). In the saline group, the median survival was only 20 days. When treated with Taxol®, tumor-bearing mice could have a longer median survival time (around 30 days). However, PTX-CPSO micelles groups significantly prolonged the median survival time of tumor-bearing mice to 40 days, suggesting that PTX-CPSO micelles were more effective to inhibit tumor growth and prolong animal survival than Taxol®. Moreover, the *in vivo* toxicity of PTX was indicated by the body weight change and organs weight change of heart, liver and kidney (Figure 7F and C). These results revealed that body weight of mice was significantly reduced when treated with Taxol®. On the contrary, the body weight exhibited a slightly increase in CPSO micelles group (1.53-fold compared to Taxol® on day 25). The heart, liver and kidney weights were not significantly changed among all groups. In addition, it has been well known that paclitaxel could induce severe toxicity to heart, live and kidney. Subsequently, these organs were sectioned to evaluate organ toxicity. As shown in Fig. 8, pathological analysis gave no evidence of morphological changes of the three major organs compared to the negative control, while nephrotoxicity involved in edema and ballooning degeneration of renal tubular epithelial cells, cytoplasmic relaxation, exudates from glomerular capsule, much smaller glomeruli of kidney and hepatotoxicity in vacuolar degeneration, respectively. These data suggested that the PTX-loaded CPSO micelles with low toxicity were safe enough for *in vivo* application.

Conclusions

In this study, we successfully developed a brain tumor-targeted drug delivery system by conjugation of cholesterol to polyoxyethylene sorbitol oleate *via* a carbonic ester linkage. The *in vitro* and *in vivo* experimental results suggested that the CPSO micelles could cross the intact BBB membrane. The novel designed CPSO micelles exhibited a remarkable stability in serum-containing buffer and tumor tissue liquid. PTX-loaded CPSO micelles also showed a great apoptosis effect on U87 human GBM cells, which was consistent with the *in vitro* test results. Further *in vivo* animal experiments indicated that CPSO micelles displayed significant tumor inhibition and prolonged the median survival times of tumor-bearing mice. The therapeutic effect of PTX-loaded CPSO micelles also demonstrated that the micelles could amply accumulate in U87 GBM. Collectively, CPSO micelles can be potentially used as a novel brain-targeted carrier which could deliver hydrophobic molecules selectively.

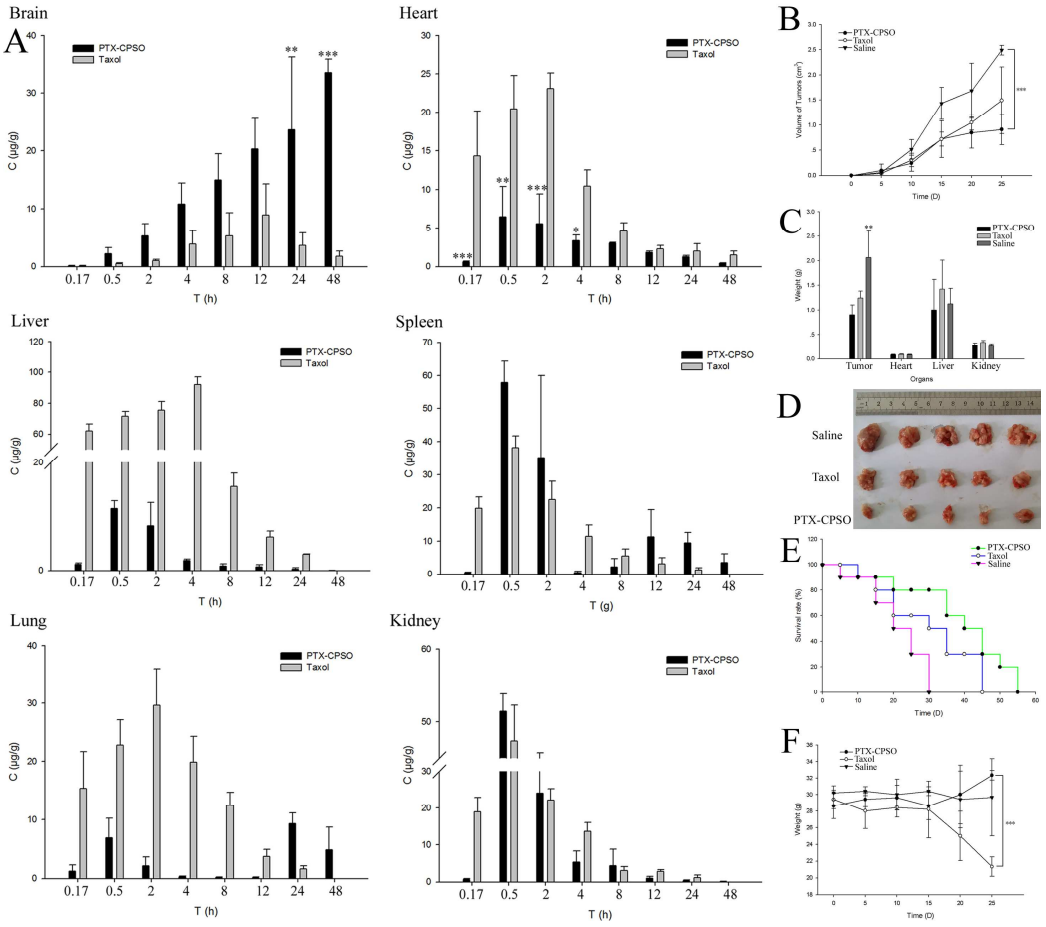

Fig. 7. Biodistribution of PTX at designated time points after i.v. injection of PTX-loaded CPSO micelles and Taxol® into normal mice. Data were given as mean ± S.D. (n = 6). *P < 0.05 versus PTX-CPSO micelles, **P < 0.01 versus PTX-CPSO micelles, ***P < 0.001 versus PTX-CPSO micelles (A). Antitumor effect in terms of tumor growth (mean ± S.D. n = 10), ***P < 0.001 (B). Tumor and other organs weight (mean ± S.D. n = 5), **P < 0.01 versus PTX-CPSO micelles (C). Tumor growth after systemic application of different drug loaded preparations (D). Survival rate (n = 10) (E). *In vivo* toxicity (in terms of body weight lost) of Taxol®, PTX-CPSO micelles and saline on tumor bearing mice after a schedule of multiple doses, ***P < 0.001, (n = 5) (F)

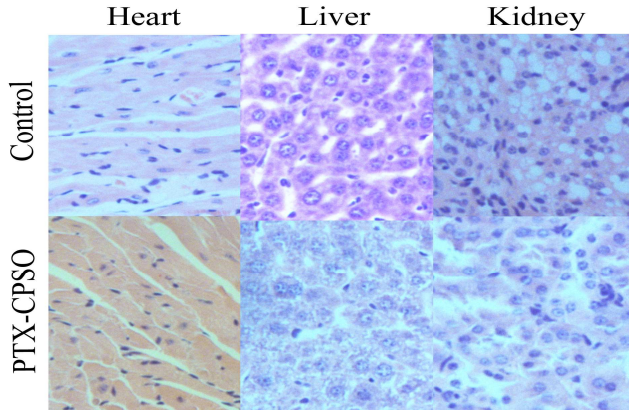

Fig. 8. Pothological sections of organs collected from tumor-bearing mices following five times i.v. injections of physiological saline and PTX-CPSO micelles.

Acknowledgements

This work was financially supported by the National Natural Science Funds for Young Scholar (No. 81201182), the Fundamental Research Funds for the Central Universities for cultivation project (No, JKPZ2013006) and the Doctoral Fund of Youth Scholars of Ministry of Education of China (No. 20130096120003). The authors wish to express their gratitude to cooperative partners from Will Chemical Co. Ltd (Nanjing, China) for their assistance in the synthesis of polyoxyethylene sorbitol oleate (PSO).

Notes and references

[a] State Key Laboratory of Natural Medicines, Department of Pharmaceutics, China Pharmaceutical University, 24 Tongjiaxiang, Nanjing 210009, China
[b] Tianjin Kingyork Group Co. Ltd., 109 Hedong district eight weft road, Tianjin 300171, China.
[c] Nanjing Sanhome Pharmaceutical Co., Ltd, Nanjing 210018, China
*Corresponding authors. Tel.: +86-25-83271305; E-mail: jiashengtu@aliyun.com (Tu J.) suncm_cpu@hotmail.com (Sun C.)
Electronic Supplementary Information (ESI) available: [details of any supplementary information available should be included here]. See DOI: 10.1039/b000000x/

1 Chen X. R, Chen L., Chen J. Y., Hu W. P., Gao H. Z., Xie B. Y., Wang X., Yin Z. L., Li S., Wang X. Y. ADAM17 promotes U87 glioblastoma stem cell migration and invasion. Brain Res. 2013, 1538, 151-158.
2 Yutaka M., Tomoya T., Kazuko T., Shourong W., Hiroshi N., Mitsunohu R. K., Yasushi I., Takahiro N., Yu M., Hiroyuki K., Horacio C., Nobuhiro N., Kazunori K. Cyclic RGD-linked polymeric micelles for targeted delivery of platinum anticancer drugs to glioblastoma through the blood-brain tumor barrier. ACS Nano. 2013, 10, 8583-8592.
3 Dalong N., Jiawen Z., Wenbo B., Huaiyong X., Fang H., Qingfeng X., Zhenwei Y., Feng C.,Qianjun H., Jianan L., Shenjian Z., Wenpei F., Liangping Z., Weijun P., Jianlin S.. Dual-targeting upconversion nanoprobes across the blood-brain barrier for magnetic resonance/fluorescence imaging of intracranial glioblastoma. ACS Nano. 2014, 2, 1231-1242.
4 Dennis R. G.. The blood-brain and blood-tumor barriers: A review of strategies for increasing drug delivery. Neuro Oncol. 2000, 1, 145-59.
5 Morteza M., Meritxell T., Ernest G.. Shuttle-mediated drug delivery to the brain. Angew. Chem. Int. Ed. 2011, 35, 7998-8014.
6 Ruirui Q., Qiaojuan J., Sabine H., Rui X., Ting L., Fabao G., Hans-Joachim G., Mingyuan G.. Receptor-mediated delivery of magnetic nanoparticles across the blood-brain barrier. ACS Nano. 2012, 4, 3304-3310.
7 Orive G., Ali O. A., Anitua E., Pedraz J. L., Emerich D. F.. Biomaterial-based technologies for brain anti-cancer therapeutics and imaging. Biochim. Biophys. Acta. 2010, 1, 96-107.
8 Y. Xiong, W. Jiang, Y. Shen, H. Li, C. Sun, A. Ouahab and J. Tu, *Biomaterials*, 2012, 33, 7182-7193.
9 C. Li, C. Sun, S. Li, P. Han, H. Sun, A. Ouahab, Y. Shen, Y. Xu, Y. Xiong and J. Tu, *International journal of nanomedicine*, 2014, 9, 2089-2100.
10 X. Ling, Y. Shen, R. Sun, M. Zhang, C. Li, J. Mao, J. Xing, C. Sun and J. Tu, *Polymer Chemistry*, 2015, DOI: 10.1039/C4PY01592D.
11 A. Ouahab, N. Cheraga, V. Onoja, Y. Shen and J. Tu, *International journal of pharmaceutics*, 2014, 466, 233-245.
12 Renad N. A., Valery E. P., Klaus L., Achim B., Dimitry A. K., Jorg K.. Delivery of Loperamide Across the Blood-Brain Barrier with Polysorbate 80-Coated Polybutylcyanoacrylate Nanoparticles. Param. Res. 1997, 14, 325-328.
13 Alexander E. G., Svetlana E. G., Igor N. S., Arkady S. A., Gregory Y. K., Jorg K.. Significant transport of doxorubicin into the brain with polysorbate 80-coated nanoparticles. Pharm. Res. 1999, 10, 1564-1569.
14 Jorg K., Peter R., Valery P., Stefan H., Svetlana E. G., Britta E., Renad A., Hagen V. B., David J. B.. Direct Evidence that Polysorbate 80-Coated Poly(Butylcyanoacrylate) Nanoparticles Deliver Drugs to the CNS via Specific Mechanisms Requiring Prior Binkding of Drug to the Nanoparticles. Pharm. Res. 2003, 20, 409-416.
15 Jean C. O., Laurence F., Romain C., Claudine P., Romeo C., William C.. Indirect Evidence that Drug Brain Targeting Using Polysorbate 80-Coated Polybutylcyanoacrylate Nanoparticles Is Related to Toxicity. Pharm. Res. 1999, 16, 1836-1842.
16 Yujun W., Cheng W., Changyang G., Yingjing W., Gang G., Feng L., Zhiyong Q.. Polysorbate 80 coated poly (ε-caprolactone)–poly (ethylene glycol)–poly (ε-caprolactone) micelles for paclitaxel delivery. Int. J. Pharm. 2012, 1-8.
17 Qiu S, Liu Z, Hou L, Li Y, Wang J, Wang H, Du W, Wang W, Qin Y, Liu Z. Complement activation associated with polysorbate 80 in beagle dogs. Int. Immunopharmacol. 2013, 15, 144-149
18 J. Descotes, C. Payen, T. Vial, Pseudo-allergic drug reactions with special reference to direct histamine release. Perspect Exp Clin Immunotoxicol, 2007, 1, 40-49.
19 Tong Y, Guan H, Wang S, Xu J, He C. Syntheses of chitin-based imprinting polymers and their binding properties for cholesterol. Carbohydr. Res. 2011, 4, 495-500.
20 Huo M, Zou A, Yao C, Zhang Y, Zhou J, Wang J, Zhu Q, Li J, Zhang Q. Somatostatin receptor-mediated tumor-targeting drug delivery using octreotide-PEG-deoxycholic acid conjugate-modified N-deoxycholic acid-O, N-hydroxyethylation chitosan micelles. Biomaterials. 2012, 27, 6393-6407.
21 Aguiar J., Carpena P., Molina-Bolivar J. A., Ruiz C. C. On the determination of the critical micelle concentration by the pyrene 1:3 ratio method. J. Colloid Interface Sci. 2003, 1, 116-122.
22 Mirjam H., Verena V. M., Kaloian K., Kerstin B., Rolf P., Rudolf Z. Amphiphilic HPMA-LMA copolymers increase the transport of Rhodamine 123 across a BBB model without harming its barrier integrity. J. Control Release. 2012, 2, 170-177.
23 Su Z, Shi Y, Xiao Y, Sun M, Ping Q, Zong L, Li S, Niu J, Huang A, You W, Chen Y, Chen X, Fei J, Tian J. Effect of octreotide surface density on receptor-mediated endocytosis in vitro and anticancer efficacy of modified nanocarrier in vivo after optimization. Int. J. Pharm. 2013, 1, 281-292.
24 Ding Y, Wang W, Feng M, Wang Y, Zhou J, Ding X, Zhou X, Liu C, Wang R, Zhang Q. A biomimetic nanovector-mediated targeted cholesterol-conjugated siRNA delivery for tumor gene therapy. Biomaterials. 2012, 34, 8893-8905.
25 Jiang T, Zhang Z, Zhang Y, Lv H, Zhou J, Li C, Hou L, Zhang Q. Dual-functional liposomes based on pH-responsive cell-penetrating peptide and hyaluronic acid for tumor-targeted anticancer drug delivery. Biomaterials. 2012, 36, 9246-9258.
26 Mo R, Sun Q, Xue J, Li N, Li W, Zhang C, Ping Q. Multistage pH-responsive liposomes for mitochondrial-targeted anticancer drug delivery. Adv. Mater. 2012, 27, 3659-3665.
27 Hou L, Yao J, Zhou J, Zhang Q. Pharmacokinetics of a paclitaxel-loaded low molecular weight heparin-all-trans-retinoid acid

conjugate ternary nanoparticulate drug delivery system. Biomaterials. 2012, 21, 5431-5440.

28 Ding Y., Wang Y., Zhou J., Gu X., Wang W., Liu C., Bao X., Wang C., Li Y., Zhang Q.. Direct cytosolic siRNA delivery by reconstituted high density lipoprotein for target-specific therapy of tumor angiogenesis. Biomaterials. 2014, 35, 7214-7227.

29 Li J, Huo M, Wang J, Zhou J, Mohammad JM, Zhang Y, Zhu Q, Waddad AY, Zhang Q. Redox-sensitive micelles self-assembled from amphiphilic hyaluronic acid-deoxycholic acid conjugates for targeted intracellular delivery of paclitaxel. Biomaterials. 2012, 7, 2310-2320.

30 Mikhail V. B., Tito F.. Molecular effects of paclitaxel: Myths and reality (A critical review). Int. J. Cancer. 1999, 2, 151-156.

31 Chunmeng Sun, Wei-Chiang Shen, Jiasheng Tu, Jennica L. Zaro. Interaction between cell-penetrating peptides and acid-sensitive anionic oligopeptides as a model for the design of targeted drug carriers. Molecular Pharmaceutics. 2014, 11(5): 1583-1590.

32 Gill I. J., Illum L., Farraj N., Ponti R. D.. Cyclodextrins as protection agents against enhancer damagen nasal delivery systems I. Assessment of effect by measurement of erythrocyte haemolysis. Eur. J. Pharm. Sci. 1994, 5, 229-236.

33 Kepan G., Xinguo J.. Influence of particle size on transport of methotrexate across blood brain barrier by polysorbate 80-coated polybutylcyanoacrylate nanoparticles. Int. J. Pharm. 2006, 1, 213-219.

34 Jorg K.. Nanoparticulate systems for brain delivery of drugs. Adv. Drug Deliv. Rev. 2001, 47, 65-81.

35 Mireia F., Lorena M. J., Mariana D. N., Shahid M. K., Chris J. J., Maria C., Volker H., Hernando A. P. Imaging of the spleen in malaria. Parasitol. Int. 2014, 1, 195-205.

36 Kathleen M. M., Ananth A., Ravi V. B. Decreased circulation time offsets increased efficacy of PEGylated nanocarriers targeting folate Ereceptors of glioma. Nanotechnology. 2007, 38, 1-11.

